In vivo imaging of Zika virus reveals dynamics of viral invasion in immune-sheltered tissues and vertical propagation during pregnancy

Ting Wang[1,2,6], Penghui Li[3,6] Yuan Zhang[1], Yan Liu[1], Zhongyuan Tan[1], Jianhong Sun[1], Xianliang Ke[1], Yuanjiu Miao[1], Dan Luo[1], Qinxue Hu[4,5], Fuqaing Xu[2,] Hanzhong Wang[1], Zhenhua Zheng[1,*]

1. CAS Key Laboratory of Special Pathogens and Biosafety, Center for Emerging Infectious Diseases, Wuhan Institute of Virology, Chinese Academy of Sciences, Wuhan 430071, China

2. Center for Brain Science, State Key Laboratory of Magnetic Resonance and Atomic and Molecular Physics, Key Laboratory of Magnetic Resonance in Biological Systems, Wuhan Center for Magnetic Resonance, Wuhan Institute of Physics and Mathematics, Chinese Academy of Sciences, Wuhan 430071, China

3. College of Life Sciences and Food Engineering, Hebei University of Engineering, Handan, China

4. State Key Laboratory of Virology, Wuhan Institute of Virology, Chinese Academy of Sciences, Wuhan 430071, China

5. Institute for Infection and Immunity, St George's, University of London, London, SW17 0RE, UK

6. These authors contributed equally to this work.

*Correspondence should be addressed to:

Zhenhua Zheng (zhengzh@wh.iov.cn)

Abstract

Rationale: Zika virus (ZIKV) is a pathogenic virus known to cause a wide range of congenital abnormalities, including microcephaly, Guillain-Barre syndrome, meningoencephalitis, and other neurological complications, in humans. This study investigated the noninvasive detection of ZIKV infection *in vivo*, which is necessary for elucidating the virus's mechanisms of viral replication and pathogenesis, as well as to accelerate the development of anti-ZIKV therapeutic strategies.

Methods: In this study, a recombinant ZIKV harbouring Nluc gene (ZIKV-Nluc) was designed, recovered, and purified. The levels of bioluminescence were directly correlated with viral loads *in vitro* and *in vivo*. The dynamics of ZIKV infection in A129 (interferon (IFN)-α/β receptor deficient), AG6 (IFN-α/β and IFN-γ receptor deficient), and C57BL/6 mice were characterized. Pregnant dams were infected with ZIKV-Nluc at E10 via intra footpad injection. Then, the pooled immune sera (anti-ZIKV neutralizing antibodies) #22-1 in ZIKV-Nluc virus-infected mice were visualized.

Results: ZIKV-Nluc showed a high genetic stability and replicated well in cells with similar properties to the wild-type ZIKV (ZIKVwt). Striking bioluminescence signals were consistently observed in animal organs, including spleen, intestine, testis, uterus/ovary, and kidney. The ileocecal junction was found to be the crucial visceral target. Infection of pregnant dams with ZIKV-Nluc showed that ZIKV was capable of crossing the maternal-fetal barrier to infect the fetuses via vertical transmission. Furthermore, it was visualized that treatment with the pooled immune sera was found to greatly restrict the spread of the ZIKV-Nluc virus in mice.

Conclusions: This study is the first to report the real-time noninvasive tracking of the progression of ZIKV invading immune-sheltered tissues and propagating vertically during pregnancy. The results demonstrate that ZIKV-Nluc represents a powerful tool for the study of the replication, dissemination, pathogenesis, and treatment of ZIKV *in vitro* and *in vivo*.

Key words: Zika virus; Bioluminescence imaging; Viscera dissemination; Tissue localization; Vertical transmission; Pooled immune sera

Introduction

Zika virus (ZIKV) is a mosquito-borne virus that belongs to the *Flaviviridae* family [1]. ZIKV was first isolated in 1947 from a febrile rhesus macaque in the Zika forest of Uganda [2]. Only 14 cases of sporadic infection with mild symptoms were reported in the following 60 years [3-5]. After several epidemics in Yap Island in 2007 and in French Polynesia and other Pacific islands in 2013-2014, ZIKV colonised the Americas in February 2015, causing 707,133 cases of autochthonous infection within 48 countries and territories by late 2016 [3, 6, 7]. During these large epidemics in the Americas, ZIKV infection resulted in severe pathological complications, notably microcephaly in newborns and Guillain-Barré syndrome (GBS) in adults [4, 6, 8]. The virus is mainly transmitted by the bite of *Aedes* mosquitoes, but direct, interhuman transmission through sexual or vertical route has also been confirmed, setting ZIKV apart from most other flaviviruses [9]. To date, there is no licensed vaccine or antiviral therapy available for the treatment of ZIKV infection. The efficient transmission of this virus combined with deficient antiviral strategies has exacerbated public panic over ZIKV [10].

The mechanisms for the dissemination and pathogenesis of ZIKV in developing fetuses, pregnant mothers, and adults remain largely unknown. ZIKV is likely to invade a unique set of immune-sheltered tissues, including the brain, testis, and placenta. Several ZIKV animal infection models have been previously established [11] to quantify viral genomes and antigens, which have provided useful information about both the viral and host factors that determine replication and pathogenesis [12-14]. However, it has not been possible to monitor the real-time patterns of ZIKV infection

through these methods [13]. The collection of tissues and organs to evaluate ZIKV infection requires the euthanasia of the animals, and important tissues or organs may be missed if samples are not taken adequately [13, 14].

Bioluminescence imaging is a sensitive and non-invasive technology that allows for the visualization of viral dynamics in real time [15, 16]. This strategy measures the light generated by luciferase-catalysed oxidation reactions, an indicator of the extent of infected tissues, by using a charge-coupled device (CCD) camera [17]. Bioluminescence imaging measures the spatial and temporal progression of both primary infection and reinfection in the same animal model, which is able to not only reduce the inter-animal variability and animal suffering, but also improve the accuracy, stability, and reproducibility of the results [18, 19]. Bioluminescence imaging has been widely utilised in the study of viruses, including influenza virus, enterovirus 71, herpes simplex virus, respiratory syncytial virus, dengue virus, Japanese encephalitis virus, monkeypox virus, and hepatitis C virus [15-17, 19-23]. Recently, bioluminescence imaging assays of flaviviruses infection in mice have been implemented using recombinant viruses harbouring the firefly luciferase (Fluc) or Renilla luciferase (Rluc) gene [19, 20, 24]. Compared with Fluc and Rluc, the very small nanoluciferase (Nluc) (19-kDa) produces 150-fold more light [17, 25], and shows a greater potential for bioluminescence imaging [26]. To date, there have been no successful attempts at the non-invasive detection of ZIKV infection *in vivo*, which is warranted for characterizing the mechanisms of the replication and pathogenesis of the virus, as well as to improve the preclinical evaluation of vaccines, antiviral drugs, or therapeutic antibodies for

ZIKV.

In this study, a recombinant ZIKV harbouring the Nluc gene (ZIKV-Nluc) was designed, recovered, and purified. This recombinant virus showed a high genetic stability and replicated well in cells with similar properties to the wild-type ZIKV (ZIKVwt). The levels of bioluminescence were found to be directly correlated with viral loads *in vitro* and *in vivo*. The dynamics of ZIKV infection in A129 (interferon (IFN)-α/β receptor deficient), AG6 (IFN-α/β and IFN-γ receptor deficient), and C57BL/6 mice were well characterized. To our knowledge, this is the first real-time non-invasive tracking of the progression of ZIKV invading immune-sheltered tissues, as well as its vertical propagating, during pregnancy. The results presented in this study demonstrate that ZIKV-Nluc is a powerful tool for use in the study of the replication, dissemination, and pathogenesis of ZIKV *in vitro* and *in vivo*.

Results

Generation and characterization of a stable reporter ZIKV

To generate a bioluminescent ZIKV reporter virus, a Nluc gene was engineered into a full-length infectious cDNA clone of an Asian-lineage Zika virus, SZ-WIV01 [10]. As shown in Figure 1A, the monomeric Nluc gene flanked by the N-terminal 38 amino acids of C protein (C38) and a FMDV2A (F2A) sequence was inserted between 5'UTR and the N-terminus of open reading frame (ORF). The C38 sequence was required for maintaining genome cyclization and for viral RNA replication. The F2A sequence was placed downstream of the Nluc gene to ensure that the Nluc protein was properly

123 processed [19, 27].

124 P0 ZIKV-Nluc virus was rescued through the transfection of Vero cells with the
125 full-length ZIKV-Nluc cDNA clone (ZIKV-Nluc-FL). P0 ZIKV-Nluc virus harbouring
126 the intact genome, without the loss of Nluc, was confirmed by RT-PCR assay by
127 amplifying the fragment from 5'UTR to the C gene (Figure 1B). Compared with
128 ZIKVwt, the P0 ZIKV-Nluc virus produced smaller plaques, which were visualized by
129 immunostaining ($P < 0.001$) (Figure 1C) and 0.33% neutral red ($P < 0.001$) (Figure 1D),
130 demonstrating that the insertion of the Nluc gene attenuated the virus in cell culture.
131 The infection of Vero cells with P0 virus resulted in the robust production of luciferase
132 activity (Figure 1E), despite the P0 virus having lower infectious titres, at 3 and 4 days
133 post infection (dpi) ($P < 0.05$), and exhibiting a lower replication efficiency than
134 ZIKVwt (Figure 1F).

135 The genetic stability of ZIKV-Nluc is prerequisite for its use. To test the stability
136 of the ZIKV-Nluc virus, the P0 ZIKV-Nluc virus was passaged in Vero cells for five
137 rounds. After each passage (P1 to P5), the viruses were examined for the Nluc gene.
138 The RT-PCR results indicated that the Nluc gene began to be lost in the P1 viral stock
139 (Figure 1G). To improve the stability of ZIKV-Nluc, the P0 ZIKV-Nluc virus was
140 purified for four rounds in Vero cells using a double plaque assay (Figure 1H). The
141 resulting P8 ZIKV-Nluc virus was re-passaged five times in Vero cells, the passages of
142 which did not result in any apparent loss of NLuc gene, indicating that the genome of
143 ZIKV-Nluc was stable for at least five life cycles (Figure 1I). Sequence analysis of the
144 entire genome of P8 ZIKV-Nluc virus revealed no nucleotide substitution (Fasta data-

S1).

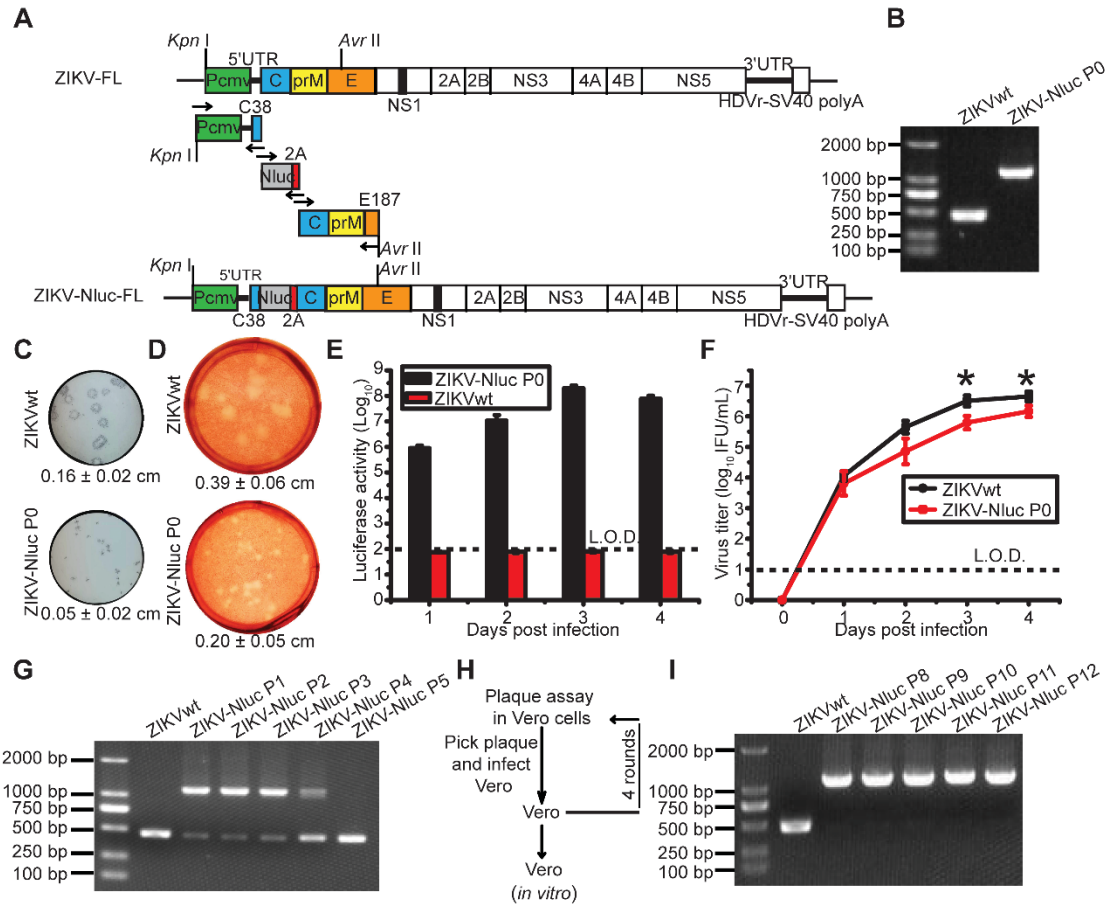

Figure 1. Generation and characterization of ZIKV-Nluc. (A) Strategy for constructing the full-length cDNA clone of ZIKV-Nluc. The monomeric Nluc gene flanked by the N-terminal 38 amino acids of C protein (C38) and a FMDV2A (F2A) sequence was inserted between 5'UTR and the C gene. (B) The stability of the P0 ZIKV-Nluc virus. Viral RNAs were extracted from the supernatants, and RT-PCR was performed with a pair of primers surrounding the Nluc-2A fragment. (C) The plaque morphology of the P0 ZIKV-Nluc virus in Vero cells, visualized by immunostaining following incubation for 4 days. (D) The plaque morphology of the P0 ZIKV-Nluc virus in Vero cells, visualized using 0.33% neutral red following incubation for 5 days. (C, D) The average sizes of viral plaques (mean ± standard deviation) were quantified by counting all of the intact plaques.

(E) Nluc activities of the infected Vero lysates by P0 ZIKV-Nluc virus at different times post infection at low multiplicity of infection (MOI) of 0.01. (F) Growth curves of P0 ZIKV-Nluc virus determined by an immunostaining plaque assay at an MOI of 0.01. (G) ZIKV-Nluc stability during virus passaging. Total RNA was extracted from the cells infected by each passaged virus, and RT-PCR was performed with a pair of primers surrounding the Nluc-2A fragment. (H) Schematic of plaque purification. (I) ZIKV-Nluc stability following plaque purification.

To further validate the ZIKV-Nluc virus (P8), viral protein synthesis was examined in Vero cells. As measured by IFA assays, the amount of E-positive cells infected with ZIKV-Nluc virus increased with the time of infection, although the percentage of positive cells was less than that of ZIKVwt before the peak at 3 dpi (Figure 2A). Next, we determined the kinetics of the luciferase activities in Vero cells infected with different MOIs (0.001, 0.01, 0.1 or 1) of ZIKV-Nluc virus. As shown in Figure 2B, the growth of the Nluc signal showed a good correlation with the MOI in the ZIKV-Nluc virus (P8)-infected Vero cells. In a parallel experiment of double plaque assay, P8 ZIKV-Nluc virus showed low infectious titres at 2, 3, 4, and 5 dpi ($P < 0.05$). However, the growth pattern for the bioluminescent virus was similar to that for ZIKVwt (Figure 2C). In addition, the MOI of 0.01 was selected and applied in subsequent correlation analyses of viral titres and Nluc activities. We demonstrated that there was an excellent linear correlation ($r^2 = 0.9114$) between the Nluc signal values and the viral titres of P8 ZIKV-Nluc virus (Figure 2D). Collectively, the P8 ZIKV-Nluc virus showed a superior genetic stability and produced levels of luciferase activity that

accurately reflected the replication of the virus *in vitro*. Therefore, this virus was used in further experiments.

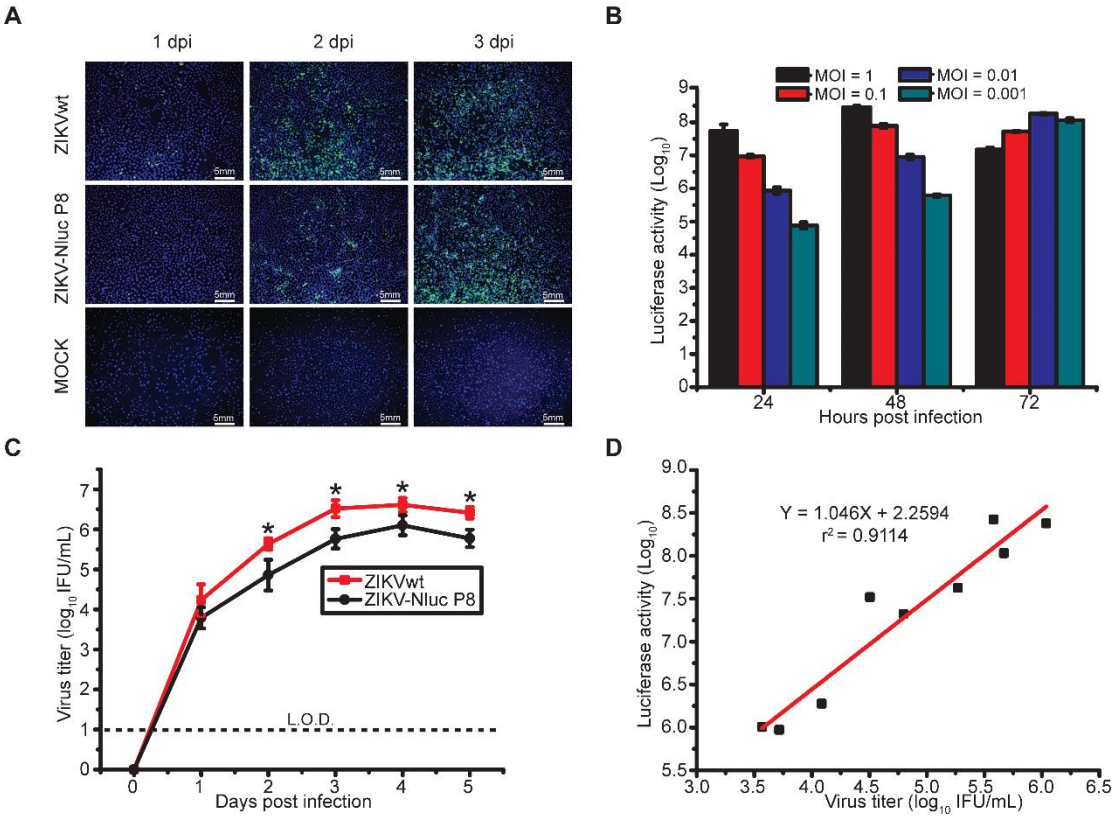

Figure 2. Replication of ZIKV-Nluc in cell culture. (A) IFA of E protein expression in Vero cells infected with the purified ZIKV-Nluc virus at an MOI of 0.05. (B) Nluc activities of infected Vero lysates by the purified ZIKV-Nluc virus at different times post infection at an MOI of 0.001, 0.01, 0.1, and 1, respectively. (C) Growth curves of the purified ZIKV-Nluc virus determined by immunostaining plaque assay at an MOI of 0.01. (D) Linear correlation between viral titres and Nluc signal values of the purified ZIKV-Nluc virus *in vitro*.

Pathogenicity of ZIKV-Nluc in A129, AG6, and C57BL/6 mice

To determine whether the ZIKV-Nluc virus causes a similar disease progression

compared to ZIKVwt, mice were infected with 1.2×10^5 IFU ZIKV-Nluc/ZIKVwt via the intraperitoneal (i.p.) route and monitored for 20 days for weight loss and mortality. Both A129 mice and AG6 mice infected with ZIKVwt showed weight loss starting at 4 dpi, and all mice died between 7 and 9 dpi (Figures 3A and B). By contrast, in the ZIKV-Nluc virus-infected mice, only 33.3% A129 mice and 50% AG6 showed significant weight loss and succumbed to infection by 19 and 18 dpi, respectively (Figures 3A and B). The immunocompetent mice, C57BL/6 mice, were not susceptible to infection with neither ZIKVwt nor ZIKV-Nluc (Figures 3A and B). The viral titres in sera obtained from A129 mice at 3 and 5 dpi were measured using an immunostaining focus assay (Figures 3C and D). A129 mice infected with ZIKV-Nluc were found to have significant different viral titres at both 3 dpi ($P < 0.05$) and 5 dpi ($P < 0.01$) compared to A129 mice infected with ZIKVwt (Figures 3C and D). These results showed that despite reduced levels of attenuation, the ZIKV-Nluc virus could develop detectable viral titres in sera, suggesting that the virus replicated well in immunodeficiency mouse models. In addition, C57BL/6 mice showed no clinical signs of disease or weight loss when infected with both ZIKV-Nluc and ZIKVwt.

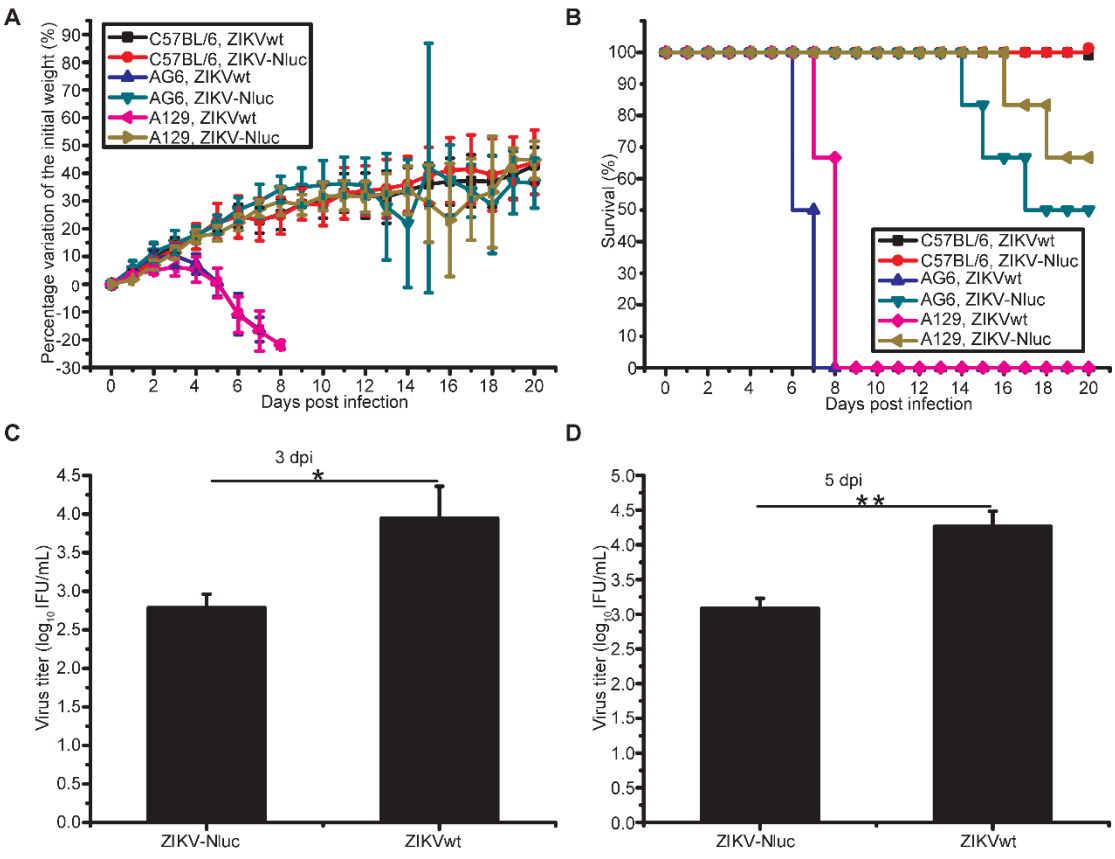

Figure 3. Pathogenicity of ZIKV-Nluc in A129, AG6, and C57BL/6 mice. (A, B) Groups of A129, AG6, and C57BL/6 mice (3-4 weeks old; n = 6) were infected intraperitoneally with 1.2×10^5 IFU of WT or ZIKV-Nluc. Body weight loss and survival were monitored on a daily basis for 20 days. (C, D) Two groups of A129 mice (3-4 weeks old; n = 3) were infected intraperitoneally with 1×10^4 IFU of WT or ZIKV-Nluc. Serum viral loads were determined at day 3 and day 5 by an immunostaining plaque assay. Data represent the mean ± SD analysed by Student's t-test (two tailed) (*, $P < 0.05$; **, $P < 0.01$).

Using ZIKV-Nluc for the bioluminescence imaging of ZIKV infection

To investigate whether ZIKV-Nluc can be used as a tool for the bioluminescence imaging of ZIKV infection, A129 mice were inoculated with 1.2×10^5 IFU ZIKV-Nluc via the i.p. route, and the bioluminescent signal was monitored at regular times post

infection. As shown in Figures 4A and B, a rapid dissemination of bioluminescence from the injection site was observed in A129 mice as early as at 1 dpi, with the peak bioluminescence occurring at 5 dpi (a robust bioluminescence signal was detected in the whole abdomen, brain, limbs, and tail). For some C57BL/6 mice, a slight detectable luminance signal above background was observed at the indicated time points (Figures 4A and B). In a separate experiment, A129 mice were inoculated intracranially (i.c.) with 6×10^3 IFU ZIKV-Nluc, and the bioluminescence in the brain regions were monitored at 2, 4, and 5 dpi. The titres of ZIKV-Nluc were measured using the double plaque assay. A direct correlation ($r^2 = 0.9617$) was found between the viral titres of ZIKV-Nluc and the intensity of luminescence, indicating that the virus replication *in vivo* could be reflected by the changes in luminescence intensity (Figures 4C and D). To further validate the correlations between the bioluminescent signals and viral loads, AG6 mice were inoculated with 6×10^4 IFU ZIKV-Nluc via the footpads. Tissues, including spleen, kidney, testis, and ileocecal junction, were isolated at 1, 3, and 5 dpi and subjected to bioluminescence imaging and viral load measurement. Linear regression analysis showed that Nluc signal values correlated well with viral RNA copies in mouse tissues (Figure S1). Collectively, using ZIKV-Nluc, the whole disease progression of the viral infection could be traced well via the IVIS CCD camera system.

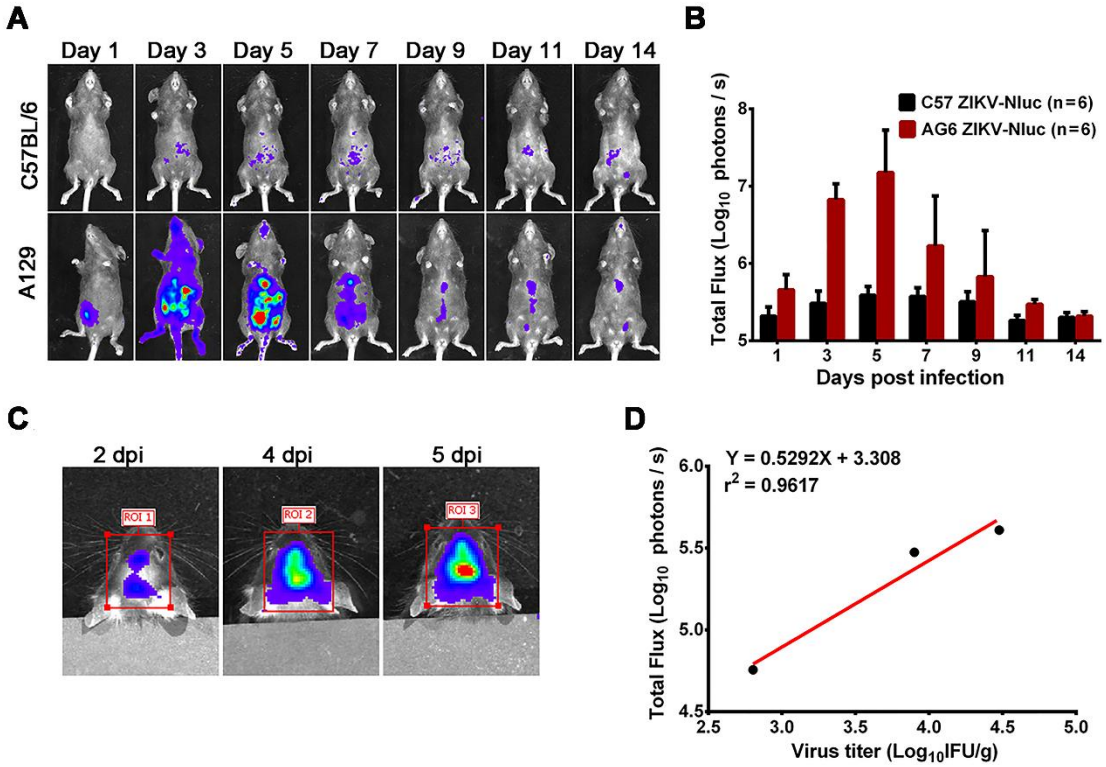

Figure 4. *In vivo* luminescence of ZIKV-Nluc-infected mice. (A, B) Groups of A129 and C57BL/6 mice (3-4 weeks old; n = 6) were infected intraperitoneally with 1.2×10^5 IFU of WT or ZIKV-Nluc. (A) Bioluminescence imaging of ZIKV-Nluc-infected mice was performed at the indicated times. Representative ventral views of the results were shown. (B) The average radiance of ZIKV-Nluc-infected mice was determined from region of interest (ROI) analysis of the ventral side. (C, D) Groups of AG6 mice (3-4 weeks old; n = 6) were infected with 6×10^3 IFU of ZIKV-Nluc via the i.c. route. (C) Bioluminescence imaging of ROI from ZIKV-Nluc-infected mice was performed at the indicated times. (D) Linear correlation between the viral titres and Nluc signal values of the ZIKV-Nluc virus *in vivo*.

Involvement of type I and type II IFN in viral dissemination

To determine the mechanisms of ZIKV dissemination and pathogenesis in adults, pregnant mothers, and developing fetuses, the infection of mouse models by mimicking

the natural infection route (footpad) is key [13, 28, 29]. A129, AG6, and C57BL/6 mice were infected with 6×10^4 IFU ZIKV-Nluc, or the parental ZIKV as control, via intra-footpad injections. The resulting bioluminescent signal was monitored longitudinally at regular time points post infection. No real or effective bioluminescence was detected in the mock-infected AG6, A129, and C57BL/6 mice, nor in mice infected with ZIKV-Nluc at 0 dpi (Figure S2). As shown in Figure 5 and Figure 6, in the infected A129 and AG6 mice, following the footpad injection, the bioluminescent signals were primarily observed at the local sites of inoculation and the peritoneal cavity at 1 dpi, further disseminating to the brain and other tissues or organs, peaking in the peritoneal cavity and brain at 5 dpi, and subsequently decreasing throughout the process of viral infection. These results revealed the complete process of ZIKV dissemination and showed that the ZIKV-Nluc virus primarily invaded various abdominal organs and the brain.

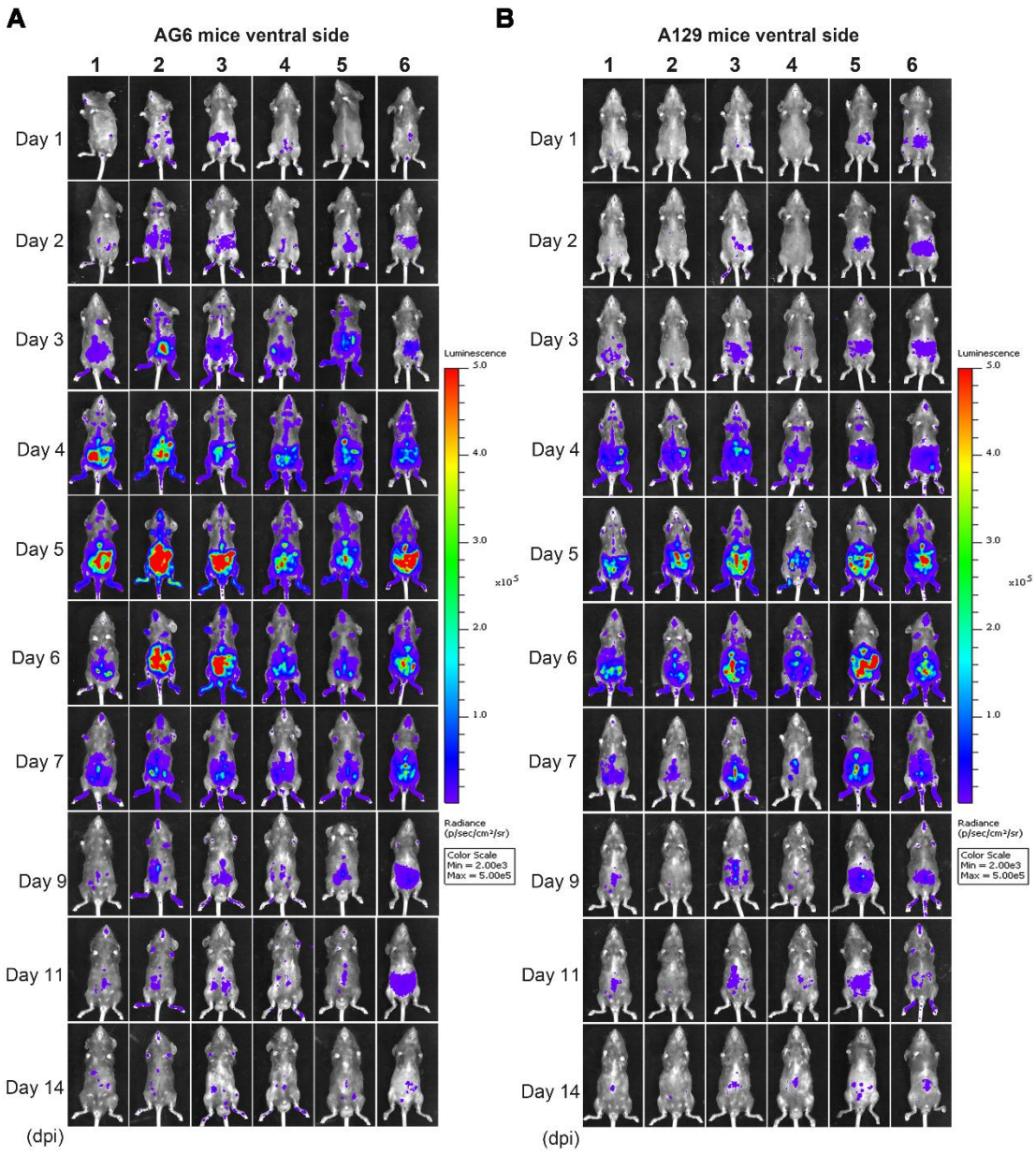

Figure 5. Spatial and temporal progression of ZIKV-Nluc in AG6 and A129 mice in ventral views. Groups of AG6 (A) and A129 (B) mice (3-4 weeks old; n = 6) were infected with 6×10^4 IFU of WT or ZIKV-Nluc via the footpad. The viral spread of ZIKV-Nluc-infected mice was monitored in real time at the indicated times.

At 9 dpi, only a slight bioluminescent signal was detected in the peritoneal cavity in the majority of the A129 and AG6 mice. However, at 14 dpi, the real and effective

bioluminescence was still detectable in the peritoneal cavity of both AG6 and A129 mice (Figure 5 and Figure 6), highlighting the viscerotropism of ZIKV *in vivo*. By contrast, only a weak bioluminescent signal was detected in the peritoneal cavity of some C57BL/6 mice almost throughout the trial period. Next, we calculated the total flux of each ZIKV-Nluc-infected mouse, and found that the signal values of the AG6 mice were significantly higher than those of the A129 mice at 2 dpi for the dorsal side ($P < 0.05$), and at 2 and 3 dpi for the ventral side ($P < 0.05$) (Figures 7A and B). These results indicated that although type I IFNs were crucial for the viscera dissemination of ZIKV-Nluc, type II IFN also played a role in the process by delaying disease development in the early stages of virus infection.

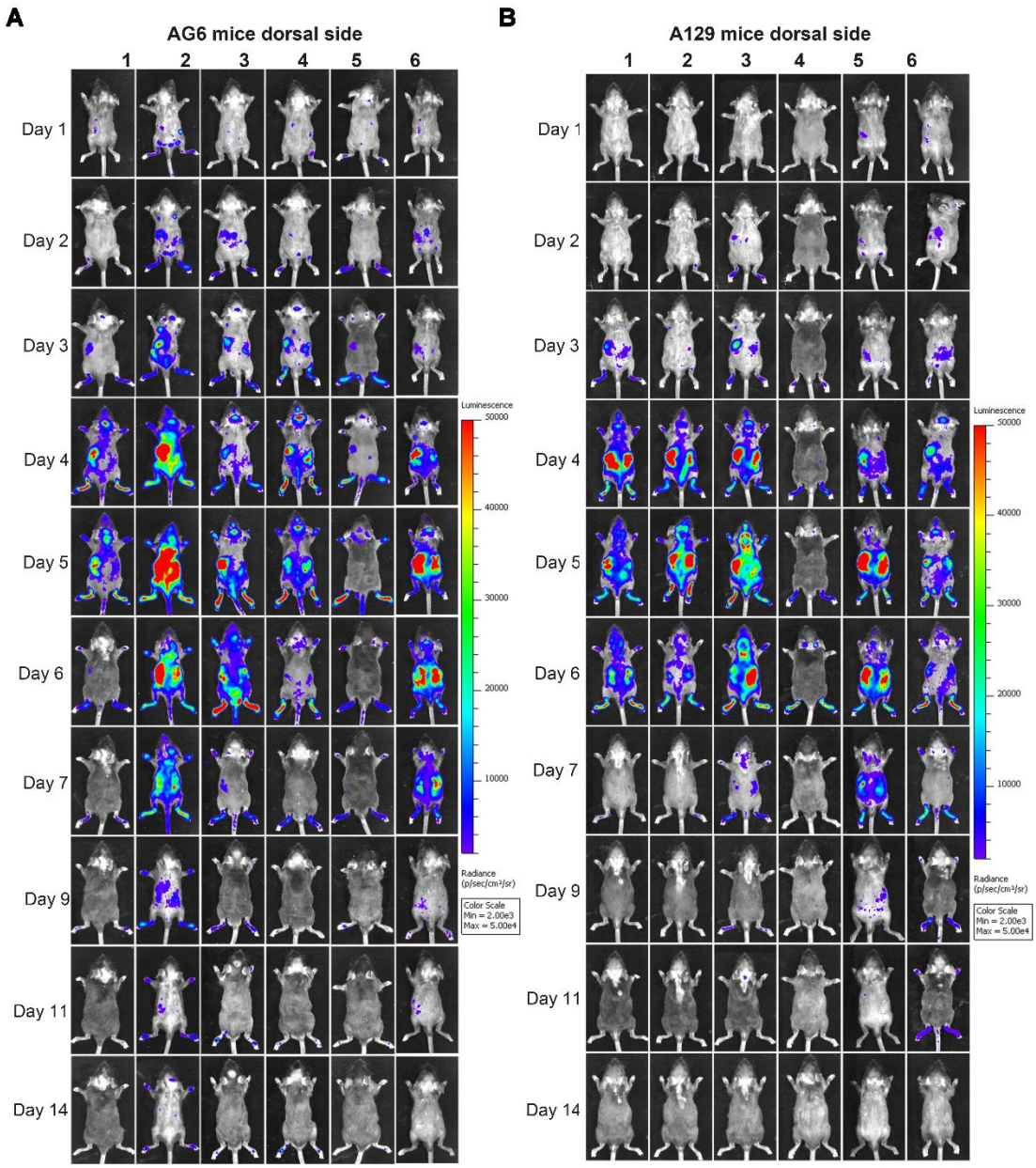

287

288 **Figure 6. Spatial and temporal progression of ZIKV-Nluc in AG6 and A129 mice in dorsal**

289 **views.** Groups of AG6 (A) and A129 (B) mice (3-4 weeks old; n = 6) were infected with 6×10^4

290 IFU of WT or ZIKV-Nluc via the footpad. The viral spread of ZIKV-Nluc-infected mice was

291 monitored in real time at the indicated times.

292

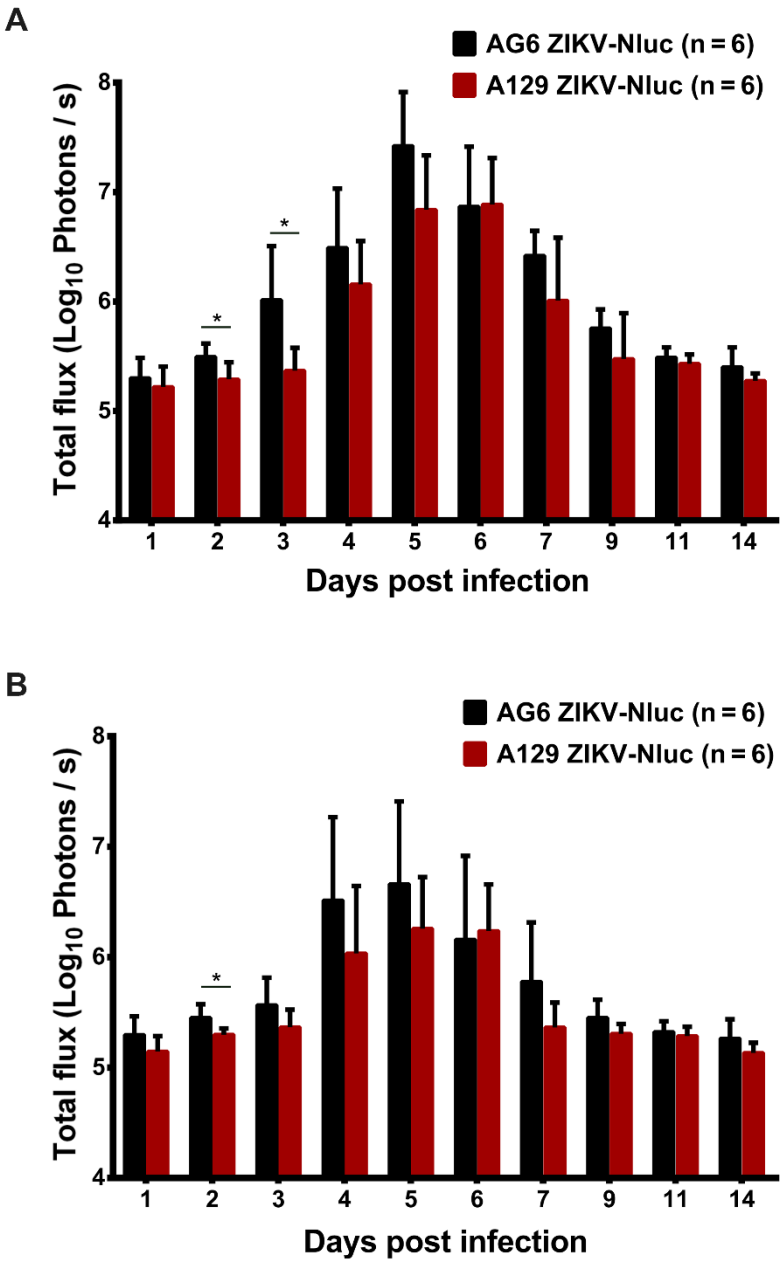

293

294 **Figure 7. Comparison of total fluxes from AG6 and A129 mice infected with ZIKV-Nluc.** (A)

295 The average radiance of AG6 and A129 mice infected with ZIKV-Nluc (mice in Figure 5 and Figure

296 6) was determined by the ROI analysis of the ventral side. (B) The average radiance of AG6 and

297 A129 mice infected with ZIKV-Nluc (Figure 5 and Figure 6) was determined by the ROI analysis

298 of the dorsal side. Data represent the mean ± SD analysed by Student's t-test (two tailed) (*, P <

299 0.05; **, P < 0.01).

300

301 **Tissue localization of ZIKV-Nluc**

302 To accurately identify the potential target organs of ZIKV-Nluc in infected mice, the *in*
303 *vitro* imaging of organs harvested from AG6, A129, and C57BL/6 mice infected with
304 ZIKV-Nluc at 3 and 5 dpi was performed in a separate experiment. Marked Nluc signals
305 were consistently observed in the abdominal organs of the infected AG6 and A129 mice,
306 including in the spleen, intestine (i.e. ileocecal junction, a key region of the intestine),
307 testis, uterus/ovary, and kidney at both time points (Figures 8A and B). Among these
308 organs, the lymphoid rich organs, namely the spleen and the ileocecal junction, radiated
309 two of the strongest light emissions, followed by the uterus/ovary, testis, and kidney.
310 Bioluminescent signals in other organs, such as the brain, heart, and lung, varied
311 individually among mice. For C57BL/6 mice, although only weak luciferase signals
312 were detected in the intestines, no detectable bioluminescence was observed in other
313 organs (Figures 8A and B). In addition, immunohistochemistry (IHC) staining of
314 ileocecal junction, testis, and brain tissue sections showed a relatively clear distribution
315 of E protein in AG6 mice infected with the ZIKV-Nluc virus (Figures 8C and D). By
316 comparison, for C57BL/6 mice, the distribution of E protein was only found in ileocecal
317 junction section at 5dpi (Figure S3). Although the possibility that infection in other
318 anatomical tissues may have occurred at earlier time points, or infected cells may have
319 migrated from one location to another at later time points, these results supported
320 previous observations that ZIKV preferentially replicated in both male and female

reproductive tracts and led to infertility in mice [12, 30].

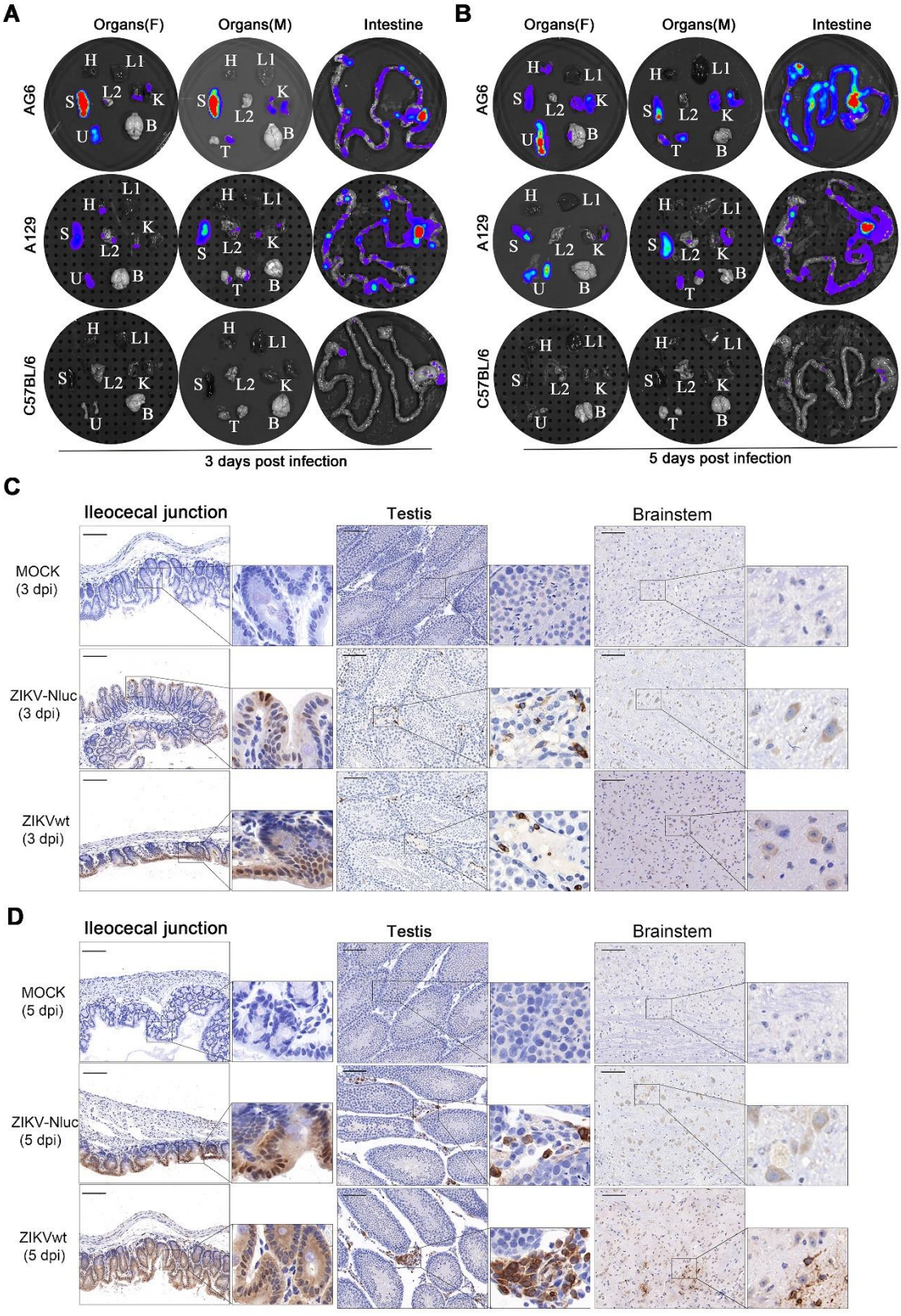

Figure 8. Tissue localization of ZIKV-Nluc. Groups of A129, AG6 and C57BL/6 mice (3-4 weeks old; n = 6) were infected with 6 ×10^4 IFU of WT or ZIKV-Nluc via footpad. Immediately after bioluminescence imaging, ZIKV-Nluc-infected mice were sacrificed, and isolated organs including heart (H), liver (L1), spleen (S), lung (L2), kidney (K), uterus/ovary (U), testis (T), and brain (B) were subjected to *in vitro* bioluminescence imaging at 3 dpi (A) and 5 dpi (B). The expressions of E protein in ileocecal junction, testis and brainstem sections from infected AG6 mice were stained by immunohistochemistry at 3 dpi (C) and 5 dpi (D). Scale bars are 100 μm for lower magnification images (× 20) and boxes in lower magnification images indicated where the higher magnification images (× 80) were taken.

Vertical transmission of ZIKV-Nluc

Given the fact that embryonic day 10-13 (E10-13, later in gestation) corresponds to the period of neurogenesis in mice [1, 31, 32], we infected pregnant dams with 6 × 10^4 IFU ZIKV-Nluc at E10 via intra-footpad injection to determine the transmission of ZIKV from mother to offspring in mice. As shown in Figure 9A, in infected pregnant AG6 mice, the bioluminescent signals were primarily detected at the local site of inoculation and in the peritoneal cavity at 1 dpi, which then disseminated to other organs before peaking at 5 dpi, decreasing steadily until delivery. By comparison, only a slight bioluminescence signal was detected in the brains of infected pregnant AG6 mice at 3 and 5 dpi, which was markedly different from that of 3-week-old AG6 mice infected with ZIKV-Nluc. The peritoneal cavity of the maternal mice still radiated slight light emissions at 1 day postpartum. In terms of the newborn mice, 25 μl of diluted substrate

via a single i.p. injection resulted in an exact and effective bioluminescence (Figure 9B), indicating that ZIKV was capable of crossing the maternal-fetal barrier to infect the fetuses through vertical transmission.

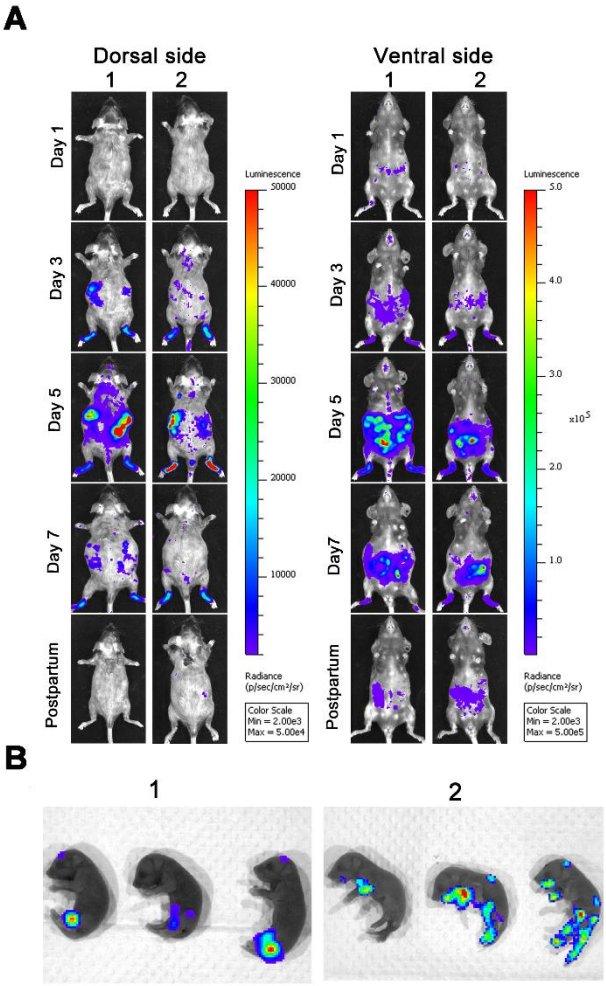

Figure 9. Spatio-temporal dynamics of ZIKV-Nluc invading pregnant mice and spreading vertically to the fetuses. Four-week-old AG6 female mice (n = 3) were mated with AG6 males. On E10, pregnant mice were infected with 6×10^4 IFU of WT or ZIKV-Nluc via the footpad. Viral spreads from the ventral and dorsal views of ZIKV-Nluc-infected pregnant mice were monitored in real time at the indicated times (A). Bioluminescence imaging of fetuses from ZIKV-Nluc-infected dams was performed at day 1 after birth (B).

Visualizing immunological protections of pooled immune serum

Although pooled immune sera (neutralizing anti-ZIKV antibodies) were recommended for protection against ZIKV infection [28, 33], it is unclear how these sera suppress the progression of viral infection *in vivo*. We adopted our established bioluminescence imaging to evaluate the immunological effect of a pooled immune serum, #22-1, which conferred robust neutralizing activities against ZIKVwt (NT_{50} titre of ~2048). Firstly, 80 IFU of the ZIKV-Nluc virus was pre-incubated with a 1:10 dilution of #22-1 at room temperature (RT) for 1.5 h before injection. The bioluminescent signal was monitored at regular time points post infection (Figure 10A). Pre-incubation with #22-1 significantly reduced the bioluminescence signal at 3 and 5 dpi (Figures 10B and C), and the bioluminescence of the #22-1-treated mice peaked in the peritoneal cavity and brain at 7 dpi (Figure 10B and Figure S4A). By contrast, the bioluminescence of the control mice peaked in the peritoneal cavity and brain at 5 dpi, before decreasing along with the process of viral infection (Figure 10B and Figure S4A).

Next, we designed a treatment regime of #22-1, as shown in Figure 10D. The pooled immune sera were administered at the indicated time points before and after infection with ZIKV-Nluc, while the bioluminescent signal was monitored at regular time points post infection. In the mice receiving PBS-immunized sera, a similar kinetic pattern of ZIKV-Nluc expression was observed in different tissues, with bioluminescence peaking at 5 dpi (Figure 10E and Figure S4B). Treatment with nine doses of #22-1 dramatically reduced the bioluminescent signal in almost all of the

infected mice (Figures 10E and F, and Figure S4B). Taken together, the #22-1 treatment greatly restricted the spread of viral infection *in vivo*, which clearly demonstrated that the ZIKV-Nluc virus could be used as a tool for the real-time monitoring of how pooled immune sera (neutralizing anti-ZIKV antibodies or antiviral compounds) suppress the progression of viral infection.

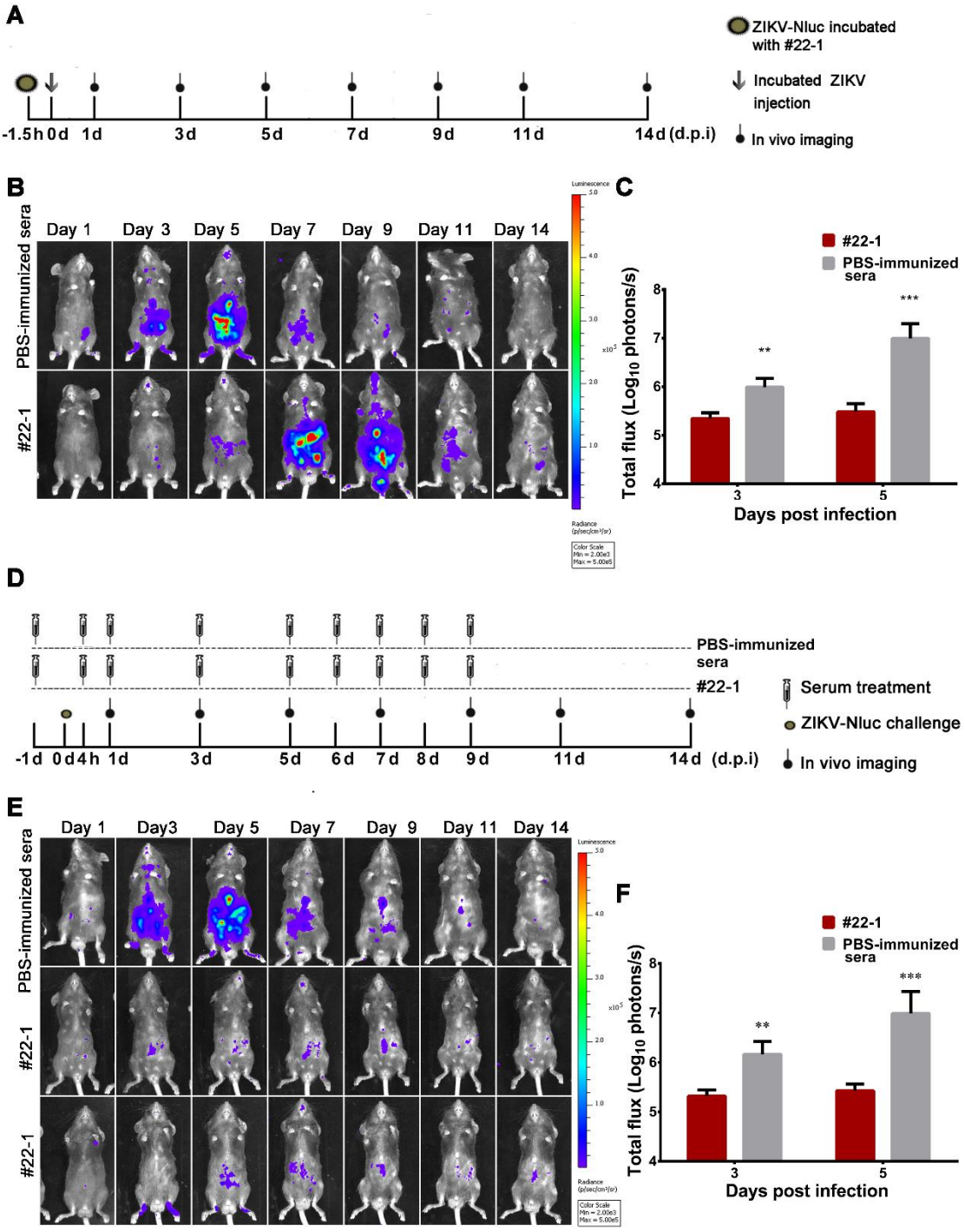

Figure 10. Application of ZIKV-Nluc for immunological protection evaluation. (A) Schematic representation of bioluminescence imaging of 3-4 weeks old AG6 mice receiving a mixture of ZIKV-Nluc and pooled immune serum, #22-1. (B) The viral spread from the ventral view of ZIKV-Nluc-infected mice was monitored in real time at the indicated times. (C) The average radiance of ZIKV-Nluc-infected mice was determined by ROI analysis of the ventral side. (D) Bioluminescence imaging of 3-4-week-old AG6 mice that received nine doses of #22-1. (E) The viral spread from the ventral view of ZIKV-Nluc-infected mice was monitored in real time at the indicated times. (F) The average radiance of ZIKV-Nluc-infected mice was determined by ROI analysis of the ventral side. Data represent the mean ± SD analysed by Student's t-test (two tailed) (*, $P < 0.05$; **, $P < 0.01$).

Discussion

ZIKV is a pathogenic virus that causes microcephaly, diffuse calcifications, GBS, meningoencephalitis, and other neurological complications in humans [4, 8, 34]. In this study, we generated a replication-competent Nluc reporter ZIKV, which is genetically stable *in vitro* and *in vivo*, which represents a powerful tool for the monitoring of the spatio-temporal dynamics of viral infection in living mice. For the first time, we report on the complete process of ZIKV dissemination, as well as the identification of the ileocecal junction as a crucial visceral target of viral infection, the tracking of the vertical propagation of ZIKV, and the congenital infection of fetuses during pregnancy. Our findings confirmed the utility of the reporter virus for use in immunological protection or therapeutic efficacy studies using mouse models.

In the generated ZIKV-Nluc virus, the Nluc reporter was expressed as an additional part of the viral polyprotein, followed by its cleavage from the capsid protein mediated by 2A protease. Notably, C38, which retained the 5' sequence downstream of the AUG region (5'DAR), the hairpin in the C protein-coding region (cHP), the 5'cyclization sequence (5'CS), and the sequence downstream of the 5'CS-pseudoknot (DCS-PK) [35-37], was duplicated upstream of the reporter gene to ensure viral RNA replication. Similar strategies have been applied in previous studies to generate several flaviviruses carrying reporter genes [27, 38-41]. A major hurdle in the practical application of these reporter flaviviruses is the relative instability of viral genomes. It has been proposed that engineered viruses evolve during their lifetime, and that a stable reporter virus could be harvested by picking small plaques [27]. In our study, a strain of P8 ZIKV-Nluc virus was found to be stable after five rounds of viral infection with no nucleotide substitution in the genome. We postulated that the high stability of P8 ZIKV-Nluc was due to the very small Nluc gene (513bp), the P0 stocks as a population (quasispecies) of general consensus sequence might contain few viral particles with mutant genomes, after purification, the single virus yields exhibited homogeneous entity and high genetic stability. Further studies are still warranted to investigate the reason for the high stability of ZIKV-Nluc. Heterologous gene insertions normally result in the attenuation of the constructed viruses both *in vitro* and *in vivo* [17, 19, 24, 41-43]. As expected, the purified ZIKV-Nluc exhibited a lower replication kinetic in the cell culture and a relatively low pathogenicity in mice. Despite this, the ZIKV-Nluc virus showed a similar growth pattern compared to that of its parental counterpart and

produced robust luciferase activities with a peak value of > 2 × 10^8 light units. The magnitude of the bioluminescence generated by ZIKV-Nluc correlated well with its titre in both the cell culture and mice, which was in agreement with the findings reported by studies on JEV and DENV reporter viruses [19, 24]. Such properties of ZIKV-Nluc provide a powerful means for further characterizing ZIKV dissemination in living mice using bioluminescence imaging.

Using the ZIKV-Nluc virus, we visualized the real-time ZIKV infection in A129, AG6, and C57BL/6 mice. ZIKV is known to directly infect neuronal progenitor cells and causes microcephaly, among other severe pathological complications [44-46]. Here, we demonstrated that ZIKV-Nluc primarily spread to the peritoneal cavity in A129, AG6, and C57BL/6 mice at 1 dpi, and was sustained throughout the remaining infection course. We hypothesized that the high viral loads in the peritoneal cavity may contribute to the quick dissemination of ZIKV to the brain and other organs. Although ZIKV-Nluc was found to be confined to specific parts of the peritoneal cavity in immunocompetent C57BL/6 mice, the lack of type I IFN receptors in A129 mice is likely to have contributed to the rapid proliferation of the virus, as well as to its spread to the brain and other organs, which was consistent with a previous biochemical analysis that found that ZIKV did not antagonize type I IFN response by promoting the degradation of STAT2 and did not induce disease in immunocompetent mice [47]. By studying genetically deficient animals, previous studies have demonstrated that type I IFNs are crucial for the dissemination of JEV to visceral organs [19]. Type I IFNs serve as one of the key components in the innate immune system, and many interferon

stimulated genes were found to be essential for viral restriction and clearance [48, 49]. After infection with a neurotropic virus, such as West Nile virus, the induction of type I IFN expression in the endothelium has been found to enhance tight junction integrity and limit the permeability of the blood–brain barrier [17, 48, 50]. We also investigated the function of type II IFNs in the control of ZIKV infection. Compared with the singly-deficient A129 mice, AG6 mice lacking both type I and type II IFN receptors were found to be more susceptible to ZIKV-Nluc, with significantly higher bioluminescent signals being observed at 2 dpi for the dorsal side and at 2 and 3 dpi for the ventral side, indicating that type II IFNs contribute to limiting systemic ZIKV infection in mice in the early stage. Neurons in the central nervous system (CNS) have a limited regeneration ability, implying that the noncytolytic clearance of virus from neuronal cells, rather than direct neuronal lysis, is required to maximize the preservation of CNS function [51]. Type II IFNs were previously found to non-cytolytically clear Sindbis virus and measles virus from infected CNS neurons [52, 53]. However, the protection of the noncytolytic immune response against neurotropic flavivirus has been disputed [51, 54]. Given that type II IFNs interact with type I IFNs through distinct as well as common IFN receptor complexes [55], we proposed that both type I and type II IFNs are functionally non-redundant for the anti-ZIKV defence, and may modulate virus dissemination by restricting infection in extraneural tissues before irreversible CNS damage in mice. Further studies will be needed to determine the exact mechanism of the non-cytolytic clearance of ZIKV from infected neurons in the CNS.

ZIKV is known to preferentially replicate in the reproductive tract, including in

the testis, uterus, and ovary [12, 30], and this has been was confirmed by the bioluminescence imaging of specific organs. However, whether the intestine is a potential target organ of ZIKV infection remains to be further clarified. In this study, we found that the Nluc signal was widespread in the whole intestine in all of the immunodeficient mice tested, indicating that the intestine is likely to serve as an important organ of ZIKV infection. Previously, luciferase signals were also detected in the intestine of singly-deficient A129 mice infected with JEV-Rluc or doubly-deficient AG129 mice infected with DENV-Fluc, suggesting that JEV and DENV can replicate in gut-associated lymphoid tissues [19, 24]. Nevertheless, it remains unclear which intestine segment is the exact ROI prone to viral infection. In this study, we excised the whole intestine of infected mice, and found that the anatomical location radiating the strongest light emission was the ileocecal junction. The ileocecal junction functions as a mechanical barrier against colonic reflux, and is involved in the “ileal brake”, which slows the transit of chyme through the intestinal tract [56, 57]. The fact that ZIKV targets the ileocecal junction is consistent with a recent study that found that the infection of enteric neurons with neurotropic flaviviruses causes delayed gastrointestinal transit in mice [58].

Our study elucidated the spatio-temporal dynamics of ZIKV in pregnant mice and its subsequent vertical spread to the fetuses. The placenta develops within days of conception and acts as an innate barrier to invading microorganisms [59, 60]. Based on epidemiological data combined with the detection of proteins and nucleic acids, it has been previously suggested that ZIKV can cross the placental barrier, being directly

associated with fetal death, microcephaly, and other fetal abnormalities during pregnancy [1, 61]. However, the mechanism for the infection and dissemination of ZIKV at the different stages of gestation remains unknown. In this study, by infecting pregnant AG6 mice with ZIKV-Nluc, the virus was found to primarily target the local site of inoculation and peritoneal cavity, subsequently spreading to other organs. The fetus may be highly sensitive to ZIKV infection during the first trimester of pregnancy [62]. However, devastating fetal outcomes, such as microcephaly, cerebral atrophy, ventricular enlargement, and cerebral calcifications, have also been found at other various gestational ages [59, 61]. Our results clearly demonstrated that the virus crossed the maternal-fetal barrier and infected newborn pups when the pregnant AG6 mice were infected at E10, corresponding to the period of neurogenesis in mice [1, 31]. Further longitudinal studies are needed in order to define the relationship between the severity of maternal infection and fetal consequences, as well as to determine the mechanism by which ZIKV crosses the placental barrier at the different stages of gestation.

We used the Nluc-expressing virus to visualize the neutralizing activities and therapeutic potential of the immune serum #22-1 in mice. As expected, significant reductions in bioluminescence signal were observed in mice receiving a pre-incubated virus-immune serum mixture in the early stages of infection. The bioluminescence in mice peaked at 9 dpi, indicating that pre-incubation before inoculation may not guarantee the neutralization of all the infectious particles. Nevertheless, these results provide new evidence for the superior genetic stability of ZIKV-Nluc *in vivo* compared with other reporter flaviviruses [19, 24]. As a proof-of-principle experiment, we traced

517 the infection and clearance of ZIKV-Nluc in A129 mice treated with several doses of
518 #22-1. The imaging results showed that a significant reduction of bioluminescence was
519 observed in the mice that received a 9-dose treatment of antiviral serum, indicating that
520 #22-1 exhibits therapeutic activity similar to that of other reported antibodies [33, 63].
521 Previously, bioluminescence imaging has been recommended to predict lethality and
522 evaluate the efficacy of vaccines and therapeutic strategies in mice [64]. Here, we
523 demonstrated that the ZIKV-Nluc virus may provide a new means for the development
524 of antiviral therapeutics and the preclinical evaluation of vaccines.

525 Despite its merits, this study also contains some limitations. One limitation was
526 that ZIKV-Nluc exhibited a lower replication efficiency and a lower pathogenicity than
527 ZIKVwt. Of note, heterologous gene insertions always led to the attenuation of
528 recombinant RNA viruses [17, 19, 24, 41-43]. Although ZIKV-Nluc was used to
529 determine the replication, dissemination, and pathogenesis of ZIKV, as well as evaluate
530 antivirals and vaccines, further studies will be needed to address the issue of attenuation.
531 The second limitation of this study was the immunocompromised mice that were used.
532 A129 and AG6 mice have been used previously to mimic aspects of ZIKV infection in
533 humans. However, due to the lack of key components of antiviral immunity, these
534 mouse models may not reveal the full range of disease manifestations in humans [11,
535 65]. Immunologically competent mice treated with IFNAR1-blocking monoclonal
536 antibody [65] or humanized mouse models may achieve better results in future studies.

537 In summary, a novel ZIKV reporter virus was established for the *in vivo* imaging
538 of ZIKV. This study is the first to investigate the spatio-temporal dynamics of ZIKV

replication, the invasion of immune-sheltered tissues by ZIKV, and the vertical propagating of ZIKV during pregnancy. In addition to the brain and reproductive tract, including the testis, uterus, and ovary, the intestine was also demonstrated to be a potential target of ZIKV dissemination, wherein the ileocecal junction may likely play a key role in the neuronal dysfunction of ZIKV infection. The non-invasive imaging of ZIKV-Nluc is a powerful tool for use in the characterisation of the replication, dissemination, and pathogenesis of ZIKV, as well as for the evaluation of antivirals and vaccines *in vivo* for the treatment of ZIKV infection in humans.

Materials and methods

Ethics statement

All animal experiments were conducted in strict accordance with the institutional guidelines for animal research and approved by the Administration of Affairs Concerning Experimental Animals of the People's Republic of China. All animal treatments were reviewed and approved in advance by the Ethics Committee of the Animal House facility of Wuhan Institute of Virology, Chinese Academy of Sciences (permit no. WIVA07201603).

Cells and viruses

African green monkey kidney epithelial cells (Vero; CCL-81; ATCC) were cultured in Dulbecco's modified Eagle's medium (DMEM) (Invitrogen, Darmstadt, Germany) containing 10% fetal bovine serum (FBS) (Life Technology, Australia), 100 U/mL

penicillin, and 100 μg/mL streptomycin maintained in 5% CO_2 at 37 °C. The parental ZIKV was rescued by transfecting Vero cells with the full-length cDNA clone, ZIKV-FL, as previously described [10].

Plasmid construction and DNA transfection

To generate the infectious clone of ZIKV-Nluc, ZIKV-FL was used as a backbone to insert the Nluc reporter gene. As shown in Figure 1A, fragment 1, covering "CMV promoter-5'UTR-C38", and fragment 3, covering "C-prM-E187", were amplified using ZIKV-FL as a template. Fragment 2, covering (Nluc-2A), was amplified using the pNL1.1 [Nluc] vector (Promega, Madison, USA) as a template. Fragments 1-3 were fused together and cloned into ZIKV-FL at the *Kpn* I and *Avr* II sites, yielding ZIKV-Nluc-FL. Before transfection, ZIKV-Nluc-FL was verified by restriction enzyme digestion and complete sequencing.

The full-length cDNA clone ZIKV-Nluc-FL under the control of the CMV promoter was used to produce infectious viruses. The transfection was performed as previously described [10]. In brief, Vero cells at 80% confluence in 35 mm culture dishes were transfected with ZIKV-Nluc-FL by lipofectamine 3000 (Life Technologies). The supernatant was harvested at 3 days post transfection (dpt), clarified by centrifugation, and stored at –80 °C.

Immunofluorescence assay (IFA)

The cells infected with ZIKVwt or ZIKV-Nluc were washed once with cold phosphate-

583 buffered saline (PBS) and fixed with cold (–20 °C) methanol–acetone (1:1) fixation
584 solution for 12 min at RT. The fixed cells were washed with PBS three times and
585 incubated with an anti-ZIKV envelope (E) protein MAb (BioFront Technologies, FL,
586 USA) (diluted 1:200) for 1 h. After washing, the cells were incubated with goat anti-
587 mouse IgG conjugated to FITC (Proteintech, Wuhan, China) (diluted 1:200) at 37 °C
588 for 60 min. After washing again, the cell nuclei were dyed with Hoechst 33258 at 37 °C
589 for 10 min. The images were photographed with a NIKON fluorescence microscope
590 (Tokyo, Japan).
591
592 **Plaque assay and immunostaining focus assay**
593 For the double plaque assay, Vero cells at 80% confluence in 6-well plates were
594 inoculated with 500 μl of 10-fold serial dilutions of viral samples in serum-free DMEM.
595 After 1.5 h incubation, 3 mL of 0.6% agarose supplemented with 2% FBS was added
596 into each well. After incubation for 4 days, 3 mL of agarose containing 0.33% neutral
597 red was added to each well. The plaques were photographed or picked after incubation
598 for another 24 h.
599 The immunostaining focus assays were performed as previously described [10].
600 In brief, Vero cells in 24-well plates were inoculated with 100 μl of 10-fold serial
601 dilutions of viral samples for 1.5 h. Then, 1 mL of 1.25% methyl cellulose overlay was
602 added to each well and the cells were incubated at 37 °C for 4 days. Cells were fixed in
603 methanol–acetone fixation solution. After washing three times, the cells were incubated
604 with ZIKV-specific hyperimmune mouse serum. After washing three more times, the

cells were incubated with HRP-conjugated second antibodies. Finally, the viral foci were visualized by addition of the DAB (3, 3-diaminobenzidine) HRP substrate using an Enhanced HRP-DAB kit (Tiangen, China), according to the manufacturer's instructions.

Luciferase assay

Vero cells at 80% confluence in 24-well plates were infected with the ZIKV-Nluc virus. After incubation in 5% CO_2 at 37 °C, the cells were lysed with passive lysis buffer at the indicated time points. Luciferase activities were measured by using the Nano-Glo® Luciferase Assay System (Promega), according to the manufacturer's instructions.

Animal experiments

The strains of mice used in this study were A129 (IFN-α/β receptor deficient), AG6 (IFN-α/β and IFN-γ receptor deficient), and C57BL/6. A129 and AG6 mice were kindly provided by Gengfu Xiao (Wuhan Institute of Virology, Chinese Academy of Sciences) and Qibin Leng (Institute Pasteur of Shanghai, Chinese Academy of Sciences), respectively. C57BL/6 mice were purchased from HuBei Center for Disease Control (CDC) (Wuhan, China). All mice were bred under specific pathogen-free conditions in the Animal Resource Center at the Wuhan Institute of Virology, Chinese Academy of Sciences.

Mice were infected with 1.2×10^5 IFU ZIKV-Nluc/ZIKVwt by intraperitoneal (i.p.) injection, or 6×10^4 IFU ZIKV-Nluc/ZIKVwt by footpad injection. PBS was injected

627 into the mock-infected mice by the same route. The clinical course of viral infection
628 was monitored by survival, weight loss, and disease symptoms.
629 For tissue localization analysis, 3-4-week-old mice that had received footpad
630 injections were anesthetized, imaged, and subjected to tissue collection (heart, liver,
631 spleen, lung, kidney, brain, testes, ovary/uterus, and intestine). All of the tissues were
632 imaged *in vitro*, then stored at –80 °C for later use. For the study of vertical transmission,
633 pregnant mice were infected at embryo day 10 (E10) by footpad injection and subjected
634 to imaging *in vivo* at the indicated time points. The newborn mice were also examined
635 by bioluminescence imaging at 1 day after birth.
636
637 **Titration of virus from excised tissues**
638 For the measurement of the viral titre, 3-4-week-old AG6 mice that that had received
639 i.c. injections were anesthetized, imaged, and subjected to tissue collection. At 2, 4, and
640 5 dpi, the brains of the infected mice were removed, weighed, and homogenized with
641 zirconia beads in 1 mL of DMEM. Then, the viral titres in the brains were quantified
642 using immunostaining focus assays.
643 For the measurement of viral loads, 3-4-week-old AG6 mice that had received
644 footpad injections were anesthetized, imaged, and subjected to tissue collection. At 1,
645 3, and 5 dpi, the spleen, kidney, testis, and ileocecal junction of the infected mice were
646 removed, weighed, and homogenized with zirconia beads in 1 mL of TRIzol reagent.
647 Next, the viral loads in tissues was quantified using qRT-PCR, as described previously
648 [10]. Briefly, the total RNA was extracted from various tissues using TRIzol reagent

649 before being reverse transcribed into cDNA by using the PrimeScript RT reagent kit. A
650 pair of primers (ZIKV-F: AARTACACATACCARAACAAAGTG and ZIKV-R:
651 TCCRCTCCCYCTYTGGTCTTG) [66] was used to amplify a conserved sequence of
652 the NS5 gene. The cycling programme comprised 95 °C for 3 min, 40 cycles of 95 °C
653 for 10 s, 55 °C for 10 s, and 65 °C for 45 s.
654
655 **Bioluminescence imaging**
656 To perform the bioluminescence imaging, the infected mice were shaved in advance
657 and anaesthetised via the subcutaneous (s.c.) injection of Avertin (150 μl/10 g of 2.5%
658 solution). The Nano-Glo substrate (Promega) was diluted 1:20 in PBS, and each mouse
659 was i.p. injected with 100 μl of the mixture. The bioluminescence data were collected
660 using an IVIS CCD camera system (Caliper Life Science), and further processed in
661 Living Image (version 4.5) software (Caliper Life Sciences). To analyse the
662 bioluminescence signals, the ROIs were selected manually in the uniformly scaled
663 images, and the data were defined as total flux in photons/second.
664
665 **Nano-Glo luminescence-based ZIKV neutralization assay**
666 A Nano-Glo luminescence-based ZIKV neutralization assay was developed for the
667 measurement of the ZIKV-specific neutralizing antibodies, according to a previously
668 described assay that used plaques as a measurement [10]. Briefly, the serum samples
669 were two-fold serially diluted, and incubated with 80 IFU of the ZIKV-Nluc virus at
670 37 °C for 1.5 h. Then, 100 μl of virus–serum mixture was added to Vero cells at 80%

671 confluence in 24-well plates. After incubation at 37 °C for 1.5 h, the cells were washed
672 once with PBS, and were then cultured in freshly prepared medium containing 2% FBS.
673 At 48 hours post infection (hpi), the levels of luciferase activity were measured using
674 the Nano-Glo® Luciferase Assay System. The 50% neutralization titre (NT_{50}) was
675 defined as the reciprocal of the highest dilution of each serum sample that resulted in a
676 50% reduction of the relative light unit relative to the control samples. The traditional
677 neutralization method, $PRNT_{50}$, was also performed to ensure the accuracy of the Nano-
678 Glo assay.
679
680 **Immunohistochemistry**
681 The immunohistochemistry assays were performed as previously described [5, 10]. In
682 brief, the tissues were fixed, embedded in paraffin, sectioned at a thickness of 5 μm,
683 and mounted onto slides. After deparaffinization and antigen retrieval, the sections were
684 incubated overnight at 4 °C. After washing three times, the sections were incubated
685 with HRP-conjugated second antibodies and visualized using DAB reagent (Envision
686 system kit; Dako). The slides were counterstained with haematoxylin and eosin. Images
687 were captured using a whole-slide digital Pannoramic scanner (3D-Histech, Budapest,
688 Hungary).
689
690 **Statistical analysis**
691 Student's t-test and analysis of variance (ANOVA) were used to analyse all of the
692 virologic and immunologic data for significant differences ($p < 0.05$). The statistical

693 analyses were performed in IBM SPSS Statistics v18.0 (Chicago, IL, USA).

694

695 ## Abbreviations

696 ZIKV, zika virus; GBS, Guillain-Barre syndrome; Fluc, firefly luciferase; Rluc, Renilla
697 luciferase; Nluc, nanoluciferase; FMDV2A, foot and mouth disease virus 2A sequence;
698 CCD, charge-coupled-device; NPCs, neuronal progenitor cell; WNV, West Nile virus;
699 CNS, central nervous system; ROI, region of interest.

700

701 ## Acknowledgments

702 The authors thank Prof. Qibin Leng of the Institute Pasteur of Shanghai, Chinese
703 Academy of Sciences for providing the AG6 mice. We would also like to thank the Core
704 Facility and Technical Support, Wuhan Institute of Virology, Chinese Academy of
705 Sciences for Xuefang An's and Fan Zhang's help in the animal experiments. This work
706 was supported by the National Key R&D Program of China (2016YFD0500406 to
707 Hanzhong Wang), National Natural Science Foundation of China (NSFC) (31800155
708 to Ting Wang, 81871665 to Yuan Zhang), and Youth Innovation Promotion Association
709 of CAS (2016302 to Zhenhua Zheng).

710

711 ## Author contributions

712 T.W., P.L. J.S, Z.T., Y.M, and D. L. performed the experiments. Y.Z, Z.Z, X.K., Y.L.,
713 and F.X performed the data analysis. T.W, P.L, and Z.Z. wrote the initial draft of the
714 manuscript. Z.Z., Q.H., and H.W revised the manuscript. All authors contributed to

715 the editing of the final version of the manuscript.

716

717 Competing Interests

718 The authors declare no competing interests.

719

720 References

721 1. Cugola FR, Fernandes IR, Russo FB, Freitas BC, Dias JL, Guimaraes KP, et al. The Brazilian Zika virus
722 strain causes birth defects in experimental models. Nature. 2016; 534: 267-71.

723 2. Dick GW, Kitchen SF, Haddow AJ. Zika virus. I. Isolations and serological specificity. Trans R Soc Trop
724 Med Hyg. 1952; 46: 509-20.

725 3. Shan C, Xie X, Shi P-Y. Zika Virus Vaccine: Progress and Challenges. Cell Host Microbe. 2018; 24: 12-
726 7.

727 4. Baud D, Gubler DJ, Schaub B, Lanteri MC, Musso D. An update on Zika virus infection. Lancet. 2017;
728 390: 2099-109.

729 5. Tan Z, Zhang W, Sun J, Fu Z, Ke X, Zheng C, et al. ZIKV infection activates the IRE1-XBP1 and ATF6
730 pathways of unfolded protein response in neural cells. J Neuroinflammation. 2018; 15: 275.

731 6. Wikan N, Smith DR. Zika virus: history of a newly emerging arbovirus. Lancet Infect Dis. 2016; 16:
732 e119-e26.

733 7. Ikejezie J, Shapiro CN, Kim J, Chiu M, Almiron M, Ugarte C, et al. Zika Virus Transmission - Region
734 of the Americas, May 15, 2015-December 15, 2016. MMWR Morb Mortal Wkly Rep. 2017; 66: 329-34.

735 8. Mlakar J, Korva M, Tul N, Popovic M, Poljsak-Prijatelj M, Mraz J, et al. Zika Virus Associated with
736 Microcephaly. N Engl J Med. 2016; 374: 951-8.

9. D'Ortenzio E, Matheron S, Yazdanpanah Y, de Lamballerie X, Hubert B, Piorkowski G, et al. Evidence of Sexual Transmission of Zika Virus. N Engl J Med. 2016; 374: 2195-8.

10. Li P, Ke X, Wang T, Tan Z, Luo D, Miao Y, et al. Zika Virus Attenuation by Codon Pair Deoptimization Induces Sterilizing Immunity in Mouse Models. J Virol. 2018; 92.

11. Morrison TE, Diamond MS. Animal Models of Zika Virus Infection, Pathogenesis, and Immunity. J Virol. 2017; 91.

12. Ma W, Li S, Ma S, Jia L, Zhang F, Zhang Y, et al. Zika Virus Causes Testis Damage and Leads to Male Infertility in Mice. Cell. 2016; 167: 1511-24.e10.

13. Dowall SD, Graham VA, Rayner E, Atkinson B, Hall G, Watson RJ, et al. A Susceptible Mouse Model for Zika Virus Infection. PLoS Negl Trop Dis. 2016; 10: e0004658.

14. Aliota MT, Caine EA, Walker EC, Larkin KE, Camacho E, Osorio JE. Characterization of Lethal Zika Virus Infection in AG129 Mice. PLoS Negl Trop Dis. 2016; 10: e0004682.

15. Rameix-Welti MA, Le Goffic R, Herve PL, Sourimant J, Remot A, Riffault S, et al. Visualizing the replication of respiratory syncytial virus in cells and in living mice. Nat Commun. 2014; 5: 5104.

16. Czakó R, Vogel L, Lamirande EW, Bock KW, Moore IN, Ellebedy AH, et al. In Vivo Imaging of Influenza Virus Infection in Immunized Mice. mBio. 2017; 8: e00714-17.

17. Caine EA, Osorio JE. In Vivo Imaging with Bioluminescent Enterovirus 71 Allows for Real-Time Visualization of Tissue Tropism and Viral Spread. J Virol. 2017; 91.

18. Cai H, Liu M, Russell CJ. Directed Evolution of an Influenza Reporter Virus To Restore Replication and Virulence and Enhance Noninvasive Bioluminescence Imaging in Mice. J Virol. 2018; 92: e00593-18.

19. Li XF, Li XD, Deng CL, Dong HL, Zhang QY, Ye Q, et al. Visualization of a neurotropic flavivirus infection in mouse reveals unique viscerotropism controlled by host type I interferon signaling.

759 Theranostics. 2017; 7: 912-25.

760 20. Li XF, Deng YQ, Zhao H, Ye Q, Wang HJ, Li SH, et al. Noninvasive bioluminescence imaging of dengue
761 virus infection in the brain of A129 mice. Appl Microbiol Biotechnol. 2013; 97: 4589-96.

762 21. Luker GD, Bardill JP, Prior JL, Pica CM, Piwnica-Worms D, Leib DA. Noninvasive bioluminescence
763 imaging of herpes simplex virus type 1 infection and therapy in living mice. J Virol. 2002; 76: 12149-61.

764 22. Wang L, Fu Q, Dong Y, Zhou Y, Jia S, Du J, et al. Bioluminescence imaging of Hepatitis C virus NS3/4A
765 serine protease activity in cells and living animals. Antiviral Res. 2010; 87: 50-6.

766 23. Falendysz EA, Londono-Navas AM, Meteyer CU, Pussini N, Lopera JG, Osorio JE, et al. Evaluation of
767 monkeypox virus infection of black-tailed prairie dogs (Cynomys ludovicianus) using in vivo
768 bioluminescent imaging. J Wildl Dis. 2014; 50: 524-36.

769 24. Schoggins JW, Dorner M, Feulner M, Imanaka N, Murphy MY, Ploss A, et al. Dengue reporter viruses
770 reveal viral dynamics in interferon receptor-deficient mice and sensitivity to interferon effectors in vitro.
771 Proc Natl Acad Sci U S A. 2012; 109: 14610-5.

772 25. Hall MP, Unch J, Binkowski BF, Valley MP, Butler BL, Wood MG, et al. Engineered luciferase reporter
773 from a deep sea shrimp utilizing a novel imidazopyrazinone substrate. ACS Chem Biol. 2012; 7: 1848-57.

774 26. England CG, Ehlerding EB, Cai W. NanoLuc: A Small Luciferase Is Brightening Up the Field of
775 Bioluminescence. Bioconjug Chem. 2016; 27: 1175-87.

776 27. Jia F, Zhu X, Xu F. A single adaptive point mutation in Japanese encephalitis virus capsid is sufficient
777 to render the virus as a stable vector for gene delivery. Virology. 2016; 490: 109-18.

778 28. Salvo MA, Kingstad-Bakke B, Salas-Quinchucua C, Camacho E, Osorio JE. Zika virus like particles
779 elicit protective antibodies in mice. PLoS Negl Trop Dis. 2018; 12: e0006210.

780 29. Jurado KA, Yockey LJ, Wong PW, Lee S, Huttner AJ, Iwasaki A. Antiviral CD8 T cells induce Zika-virus-

781 associated paralysis in mice. Nat Microbiol. 2018; 3: 141-7.

782 30. Carroll T, Lo M, Lanteri M, Dutra J, Zarbock K, Silveira P, et al. Zika virus preferentially replicates in

783 the female reproductive tract after vaginal inoculation of rhesus macaques. PLoS Pathog. 2017; 13:

784 e1006537.

785 31. Finlay BL, Darlington RB. Linked regularities in the development and evolution of mammalian

786 brains. Science. 1995; 268: 1578-84.

787 32. Miner JJ, Diamond MS. Zika Virus Pathogenesis and Tissue Tropism. Cell Host Microbe. 2017; 21:

788 134-42.

789 33. Sapparapu G, Fernandez E, Kose N, Bin C, Fox JM, Bombardi RG, et al. Neutralizing human

790 antibodies prevent Zika virus replication and fetal disease in mice. Nature. 2016; 540: 443-7.

791 34. Song BH, Yun SI, Woolley M, Lee YM. Zika virus: History, epidemiology, transmission, and clinical

792 presentation. J Neuroimmunol. 2017; 308: 50-64.

793 35. Yun SI, Lee YM. Zika virus: An emerging flavivirus. J Microbiol. 2017; 55: 204-19.

794 36. Friebe P, Shi PY, Harris E. The 5' and 3' downstream AUG region elements are required for

795 mosquito-borne flavivirus RNA replication. J Virol. 2011; 85: 1900-5.

796 37. Liu ZY, Li XF, Jiang T, Deng YQ, Zhao H, Wang HJ, et al. Novel cis-acting element within the capsid-

797 coding region enhances flavivirus viral-RNA replication by regulating genome cyclization. J Virol. 2013;

798 87: 6804-18.

799 38. Gadea G, Bos S, Krejbich-Trotot P, Clain E, Viranaicken W, El-Kalamouni C, et al. A robust method

800 for the rapid generation of recombinant Zika virus expressing the GFP reporter gene. Virology. 2016;

801 497: 157-62.

802 39. Mutso M, Saul S, Rausalu K, Susova O, Zusinaite E, Mahalingam S, et al. Reverse genetic system,

803 genetically stable reporter viruses and packaged subgenomic replicon based on a Brazilian Zika virus
804 isolate. J Gen Virol. 2017; 98: 2712-24.
805 40. Shan C, Xie X, Muruato Antonio E, Rossi Shannan L, Roundy Christopher M, Azar Sasha R, et al. An
806 Infectious cDNA Clone of Zika Virus to Study Viral Virulence, Mosquito Transmission, and Antiviral
807 Inhibitors. Cell Host Microbe. 2016; 19: 891-900.
808 41. Zou G, Xu HY, Qing M, Wang QY, Shi PY. Development and characterization of a stable luciferase
809 dengue virus for high-throughput screening. Antiviral Res. 2011; 91: 11-9.
810 42. Manicassamy B, Manicassamy S, Belicha-Villanueva A, Pisanelli G, Pulendran B, Garcia-Sastre A.
811 Analysis of in vivo dynamics of influenza virus infection in mice using a GFP reporter virus. Proc Natl
812 Acad Sci U S A. 2010; 107: 11531-6.
813 43. Pan W, Dong Z, Li F, Meng W, Feng L, Niu X, et al. Visualizing influenza virus infection in living mice.
814 Nat Commun. 2013; 4: 2369.
815 44. Yuan L, Huang XY, Liu ZY, Zhang F, Zhu XL, Yu JY, et al. A single mutation in the prM protein of Zika
816 virus contributes to fetal microcephaly. Science. 2017.
817 45. Tang H, Hammack C, Ogden SC, Wen Z, Qian X, Li Y, et al. Zika Virus Infects Human Cortical Neural
818 Progenitors and Attenuates Their Growth. Cell Stem Cell. 2016; 18: 587-90.
819 46. Garcez PP, Loiola EC, Madeiro da Costa R, Higa LM, Trindade P, Delvecchio R, et al. Zika virus impairs
820 growth in human neurospheres and brain organoids. Science. 2016; 352: 816-8.
821 47. Grant A, Ponia SS, Tripathi S, Balasubramaniam V, Miorin L, Sourisseau M, et al. Zika Virus Targets
822 Human STAT2 to Inhibit Type I Interferon Signaling. Cell Host Microbe. 2016; 19: 882-90.
823 48. Daniels BP, Klein RS. Knocking on Closed Doors: Host Interferons Dynamically Regulate Blood-Brain
824 Barrier Function during Viral Infections of the Central Nervous System. PLoS Pathog. 2015; 11: e1005096.

825 49. McNab F, Mayer-Barber K, Sher A, Wack A, O'Garra A. Type I interferons in infectious disease. Nat
826 Rev Immunol. 2015; 15: 87-103.
827 50. Daniels BP, Holman DW, Cruz-Orengo L, Jujjavarapu H, Durrant DM, Klein RS. Viral pathogen-
828 associated molecular patterns regulate blood-brain barrier integrity via competing innate cytokine
829 signals. mBio. 2014; 5: e01476-14.
830 51. Prestwood TR, Morar MM, Zellweger RM, Miller R, May MM, Yauch LE, et al. Gamma interferon
831 (IFN-gamma) receptor restricts systemic dengue virus replication and prevents paralysis in IFN-
832 alpha/beta receptor-deficient mice. J Virol. 2012; 86: 12561-70.
833 52. Binder GK, Griffin DE. Interferon-gamma-mediated site-specific clearance of alphavirus from CNS
834 neurons. Science. 2001; 293: 303-6.
835 53. Patterson CE, Lawrence DM, Echols LA, Rall GF. Immune-mediated protection from measles virus-
836 induced central nervous system disease is noncytolytic and gamma interferon dependent. J Virol. 2002;
837 76: 4497-506.
838 54. Shrestha B, Wang T, Samuel MA, Whitby K, Craft J, Fikrig E, et al. Gamma interferon plays a crucial
839 early antiviral role in protection against West Nile virus infection. J Virol. 2006; 80: 5338-48.
840 55. Lasfar A, Cook JR, Cohen Solal KA, Reuhl K, Kotenko SV, Langer JA, et al. Critical role of the
841 endogenous interferon ligand-receptors in type I and type II interferons response. Immunology. 2014;
842 142: 442-52.
843 56. Degen LP, von Flue MO, Collet A, Hamel C, Beglinger C, Harder F. Ileocecal segment transposition
844 does not alter whole gut transit in humans. Ann Surg. 1997; 226: 746-51; discussion 51-2.
845 57. Barreto SG, Windsor JA. Does the Ileal Brake Contribute to Delayed Gastric Emptying After
846 Pancreatoduodenectomy? Dig Dis Sci. 2017; 62: 319-35.

847 58. White JP, Xiong S, Malvin NP, Khoury-Hanold W, Heuckeroth RO, Stappenbeck TS, et al. Intestinal
848 Dysmotility Syndromes following Systemic Infection by Flaviviruses. Cell. 2018; 175: 1198-212.e12.
849 59. Coyne CB, Lazear HM. Zika virus - reigniting the TORCH. Nat Rev Microbiol. 2016; 14: 707-15.
850 60. El Costa H, Gouilly J, Mansuy JM, Chen Q, Levy C, Cartron G, et al. ZIKA virus reveals broad tissue
851 and cell tropism during the first trimester of pregnancy. Sci Rep. 2016; 6: 35296.
852 61. Brasil P, Pereira JP, Jr., Moreira ME, Ribeiro Nogueira RM, Damasceno L, Wakimoto M, et al. Zika
853 Virus Infection in Pregnant Women in Rio de Janeiro. N Engl J Med. 2016; 375: 2321-34.
854 62. Johansson MA, Mier-y-Teran-Romero L, Reefhuis J, Gilboa SM, Hills SL. Zika and the Risk of
855 Microcephaly. N Engl J Med. 2016; 375: 1-4.
856 63. Zhao H, Fernandez E, Dowd KA, Speer SD, Platt DJ, Gorman MJ, et al. Structural Basis of Zika Virus-
857 Specific Antibody Protection. Cell. 2016; 166: 1016-27.
858 64. Zaitseva M, Kapnick SM, Scott J, King LR, Manischewitz J, Sirota L, et al. Application of
859 bioluminescence imaging to the prediction of lethality in vaccinia virus-infected mice. J Virol. 2009; 83:
860 10437-47.
861 65. Lazear HM, Govero J, Smith AM, Platt DJ, Fernandez E, Miner JJ, et al. A Mouse Model of Zika Virus
862 Pathogenesis. Cell Host Microbe. 2016; 19: 720-30.
863 66. Faye O, Faye O, Diallo D, Diallo M, Weidmann M, Sall AA. Quantitative real-time PCR detection of
864 Zika virus and evaluation with field-caught mosquitoes. Virol J. 2013; 10: 311.
865